

Approximate Imitation Learning for Event-based Quadrotor Flight in Cluttered Environments

Nico Messikommer, Jiaxu Xing, Leonard Bauersfeld, Marco Cannici, Elie Aljalbout, Davide Scaramuzza
Robotics and Perception Group, University of Zurich, Switzerland.

Abstract—Event cameras offer high temporal resolution and low latency, making them ideal sensors for high-speed robotic applications where conventional cameras suffer from image degradations such as motion blur. In addition, their low power consumption can enhance endurance, which is critical for resource-constrained platforms. Motivated by these properties, we present a novel approach that enables a quadrotor to fly through cluttered environments at high speed by perceiving the environment with a single event camera. Our proposed method employs an end-to-end neural network trained to map event data directly to control commands, eliminating the reliance on standard cameras. To enable efficient training in simulation, where rendering synthetic event data is computationally expensive, we propose *Approximate Imitation Learning*, a novel imitation learning framework. Our approach leverages a large-scale offline dataset to learn a task-specific representation space. Subsequently, the policy is trained through online interactions that rely solely on lightweight, simulated state information, eliminating the need to render events during training. This enables the efficient training of event-based control policies for fast quadrotor flight, highlighting the potential of our framework for other modalities where data simulation is costly or impractical. Our approach outperforms standard imitation learning baselines in simulation and demonstrates robust performance in real-world flight tests, achieving speeds up to 9.8 ms^{-1} in cluttered environments.

Index Terms—Event Cameras, Quadrotors, Imitation Learning.

I. INTRODUCTION

Standard cameras capture dense visual information of the environment, enabling impressive robot performance across a wide range of applications [1]–[3]. However, their performance significantly degrades during high-speed motion due to motion blur. Since standard cameras integrate incoming light over a finite exposure time, any motion during this period results in blurred images. As a consequence, the quality of perception algorithms deteriorates significantly, which negatively affects the downstream robot policy.

Event cameras offer a radically different sensing mechanism inspired by the biological vision system [4]. Instead of integrating the incoming light, each pixel in an event camera asynchronously triggers events if the change in intensity exceeds a given threshold, called the contrast threshold. The asynchronous triggering of events reduces the sensing latency to the order of microseconds, compared to standard cameras that operate at fixed frame rates around 20 Hz. As a result, they provide sharp visual information even in fast motions

This work was supported by the European Union’s Horizon Europe Research and Innovation Programme under grant agreement No. 101120732 (AUTOASSESS), and the European Research Council (ERC) under grant agreement No. 864042 (AGILEFLIGHT).

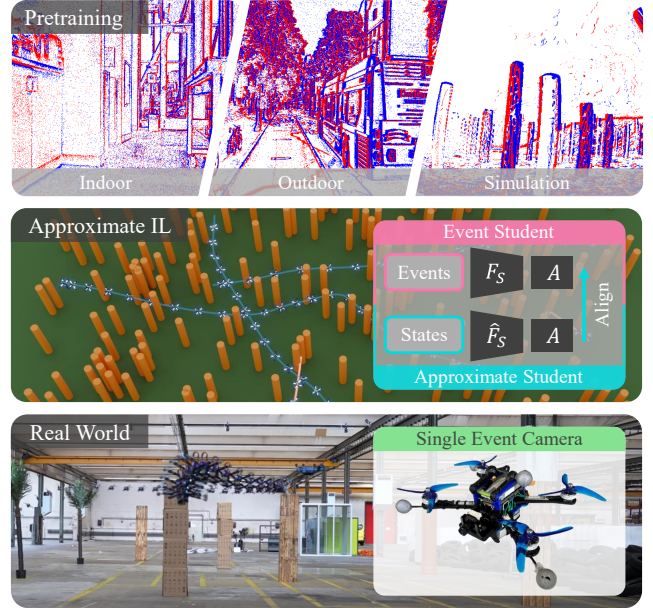


Fig. 1. **Overview of Our Proposed Framework.** Our proposed framework leverages a large-scale offline dataset of rendered events alongside a real-world dataset covering diverse scenes. To fine-tune the event-based policy, we introduce an approximate student that receives efficiently simulated state information, entirely eliminating the need for computationally expensive event rendering. We validate our framework by flying a quadrotor equipped with a single event camera through cluttered real-world environments using external pose information.

with low latency. Furthermore, event cameras excel in scenes with very large brightness variations since they feature a high dynamic range that exceeds 120 dB. These properties make event cameras an ideal choice to capture scene information reliably in high-speed robotic tasks.

An important application benefiting from the reliable perception in high-speed motion is autonomous quadrotor flight in cluttered environments, such as forests. An example is time-sensitive missions, such as search and rescue missions, where rapid and reliable navigation through complex terrain can become life-saving. Although prior work using standard cameras has shown promising results in such environments [5], they remain fundamentally limited by motion blur at high speeds. An emerging direction to tackle this downside is the solution of mounting a LiDAR sensor on a quadrotor [6]. While already smaller in scale, LiDAR sensors still have a high cost and a heavier weight. Finally, methods using event cameras to increase sensing robustness have been proposed [7], [8]. However, most of them use a standard camera to control

the quadrotor and can additionally rely on an intermediate representation, which introduces computational overhead [8].

In our work, we propose an end-to-end approach, which maps events directly to commands without any intermediate representation or standard cameras, see Fig. 1. This has the great benefit that the method can directly leverage the high-temporal resolution of the event camera for fast quadrotor flight. During training, to avoid the high computational cost of rendering high-frequency event data, our method first learns a task-relevant representation space from large-scale offline event datasets. This learned representation is then used within a lightweight simulator to train the control policy via the action decoder. Crucially, the learning of the behavior does not rely on rendering events, making it highly efficient.

The results in simulation confirm the effectiveness of our proposed *approximate Imitation Learning (IL)* framework. Our method achieves a success rate increase of 0.2 compared to the behavior cloning baseline and an increase of 0.7 to the DAgger [9] baseline. By leveraging the approximate student, our approach significantly reduces training costs, accelerating policy training by a factor of 28. Finally, we validate our approach in the real world, where the quadrotor achieves speeds up to 9.8 m s^{-1} using external state information. Although we apply our method only to event data, the framework is broadly applicable and can easily be extended to other modalities, which are computationally expensive to simulate, e.g., tactile sensors, radar, or LiDAR.

II. RELATED WORKS

A. Efficient Robot Learning

Achieving agile and robust control with limited real-world data remains a fundamental challenge in robot learning. Reinforcement learning (RL) provides a general framework for acquiring high-performance controllers through trial and error, and has demonstrated success in both simulated [10] and real-world settings [11]–[14]. However, RL methods typically suffer from low sample efficiency and high computational demands, particularly when learning directly from high-dimensional sensory inputs such as images or event streams. To improve data efficiency, imitation learning (IL) offers a compelling alternative by leveraging expert demonstrations to initialize or guide policy learning, thereby reducing the need for costly or unsafe exploration [15]–[17]. Despite its advantages, IL still faces limitations: even advanced variants such as DAgger [9], which aim to mitigate covariate shift during execution, often require substantial interaction to generalize effectively in complex or dynamic environments. A complementary direction to further reduce sample complexity targets the perception module. Instead of learning visual representations from scratch, recent approaches increasingly rely on pretrained encoders to extract rich, transferable features that can accelerate policy learning and improve generalization [18]–[20]. Together, these advances point to a promising direction: combining IL from expert demonstration with pretrained or fine-tuned visual backbones to achieve sample-efficient visuomotor control. In this work, we build upon this paradigm and propose an approximate imitation learning

framework for agile and low-latency quadrotor navigation in cluttered environments.

B. Event-Based Quadrotor Flight

Event cameras have gained popularity in robotics for their high temporal resolution and low-latency output [21]–[23]. These qualities are especially beneficial for agile autonomous flight, where rapid reaction times are critical. Early efforts in this space focused on handcrafted pipelines optimized for minimal latency. For instance, Falanga et al. [7] used event data for dynamic obstacle avoidance with a quadrotor, achieving a control loop latency of 3.5 ms. Subsequent approaches moved toward learning-based controllers to improve generalization and adaptability. Some works leveraged spiking neural networks (SNNs), which naturally align with the asynchronous nature of event data. For example, Vitale et al. [24] demonstrated line tracking on a constrained dualcopter platform using an SNN, while Paredes-Vallés et al. [23] extended this concept to unconstrained drone flight, achieving real-time ego-motion estimation and control with successful sim-to-real transfer. Other works adopted conventional deep neural networks (DNNs) for learning from event data. Andersen et al. [25] trained a perception system for high-speed gate detection in drone racing, while Zhang et al. [26] combined event streams with depth data for object tracking and navigation in cluttered environments. Most related to our work is Bhattacharya et al. [8], who trained an event-based policy in simulation via teacher-student distillation. While effective, their approach relies on approximate event renderings with limited temporal resolution during training, which can restrict the fidelity of temporal dynamics. In contrast, we first learn a task-specific representation space from offline data, and then rely on an approximate student that uses state information to simulate the event-driven behavior, avoiding event rendering entirely.

C. Vision-Based Quadrotor Flight

Autonomous quadrotor navigation in cluttered environments often depends solely on onboard visual sensing, particularly in the absence of external localization systems [27], [28]. Traditional model-based approaches tackle this challenge by estimating the quadrotor state using visual-inertial odometry (VIO) [29], [30], followed by separate control and planning modules [31], [32]. While effective in structured settings, these pipelines often suffer from brittle state estimation, delayed reaction times, and limited adaptability, making them unsuitable for agile maneuvers in dynamic or perceptually degraded environments. To address the challenge of vision-based quadrotor navigation, an early application of reinforcement learning is [33], where a policy trained in a CAD-based simulation outputs discrete velocity commands. This method assumes onboard attitude stabilization and still relies on VIO for state estimation. Subsequent methods [16], [34]–[37] learn to predict high-level control commands directly from visual observations. However, these approaches are primarily tailored to tasks such as image-goal navigation or obstacle avoidance, and typically lack the responsiveness required for agile flight in

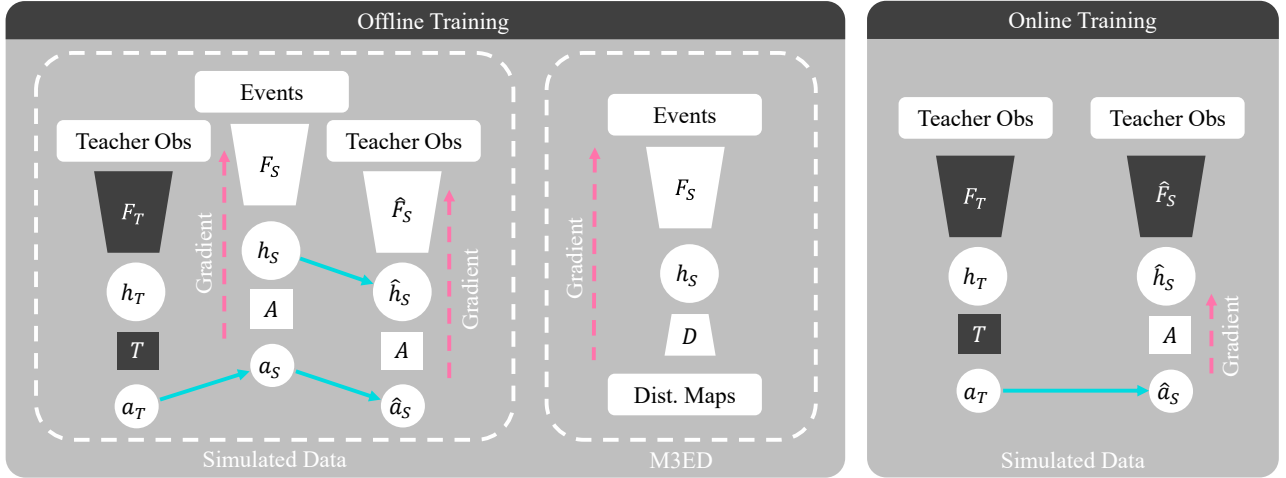


Fig. 2. **Approximate Imitation Learning Overview.** During offline training, teacher actions a_T supervise the event student by updating its encoder F_S and the shared action decoder A . The state-based approximate student, using teacher observations, is trained by aligning its features h_S and actions \hat{a}_S with the student features h_S and actions a_S , without backpropagating through the forward pass of the student. Distance maps generated from M3ED [45] serve as targets for updating the event encoder F_S and an auxiliary decoder D , adapting the event feature space h_S to real-world events. During online training, teacher observations obtained from lightweight simulations are used to fine-tune the behavior of the approximate student by updating the shared action decoder A , implicitly improving the behavior of the event student. For clarity, the auxiliary decoder D_o and the offline data update during online training are omitted.

cluttered environments. To fully exploit the potential of vision-based learning, more recent methods predict low-level control commands directly from images, enabling tighter perception-action coupling for agile maneuvers. Notably, Kaufmann et al. [38] developed a system that integrates VIO with a reinforcement learning (RL) policy, trained in simulation and fine-tuned using motion-capture data, which outperformed world champion pilots in a fair drone race. Building upon this, recent works [39]–[41] have demonstrated that agile flight can be achieved without relying on any explicit state estimation, relying on vision-based RL. In parallel to RL, IL has proven highly effective for vision-based quadrotor control. Most IL methods minimize the behavioral discrepancy between a learned policy and expert demonstrations [9], [42], resulting in significantly improved sample efficiency. This advantage has enabled IL to be successfully applied to agile flight using end-to-end visuomotor policies [20], [43], [44]. However, even with techniques such as DAgger [9], these approaches often require millions of interaction samples in simulation to achieve robust performance. This inefficiency becomes particularly problematic when considering event-based vision as the primary sensing modality, since rendering and processing event streams is computationally expensive. As a result, improving sample efficiency becomes a central requirement for enabling event-based visuomotor learning. In this work, we address this limitation by applying approximate imitation learning to further reduce sample complexity and make event-driven agile flight more tractable.

III. METHODOLOGY

A. Obstacle Avoidance Task

To evaluate the advantages of event cameras for agile robot navigation, we consider the challenging task of high-speed quadrotor flight in cluttered environments. The objective in this

setting is to navigate the quadrotor safely through obstacle-dense environments while simultaneously pushing the limits of perception by maximizing flight speed. As an external guidance signal, the policy receives a commanded direction with a magnitude corresponding to the target velocity, which it tries to track while simultaneously avoiding obstacles.

B. Approximate Imitation Learning

To efficiently train an end-to-end policy using events, we adopt a two-stage learning approach that separates representation learning from policy search, as illustrated in Fig. 2. In the first stage, we train a mapping from events to a representation space using a pre-rendered offline dataset consisting of paired event representations and teacher actions. To ensure that the learned representation space covers task-relevant information, we apply a Behavior Cloning objective based on the actions of the teacher. We additionally incorporate a real-world event camera dataset to train on an auxiliary depth task to improve generalization and robustness. However, it is well known that offline Behavior Cloning struggles when the training data does not adequately cover the state distribution encountered during real-world execution. To address this, we introduce a second stage that includes online student interaction in a simulator, crucially, without rendering events. Instead, we use an approximate student model that observes full state information and learns to mimic the actions of the event-based student, which is inspired by [46]. These interactions allow us to adapt the shared action decoder to a broader state distribution while avoiding the high computational cost of event rendering. In the following sections, we provide a detailed explanation of each training stage and the structure of the network components.

1) *Offline Training:* The offline dataset is generated by rolling out the expert teacher policy for 40,000 steps across 25

parallel environments. To increase the diversity of the state-action distribution, we apply small stochastic perturbations to the actions of the teacher during rollout. A key advantage of this approach is that the expensive event rendering is performed only once, making the dataset reusable. This dataset is then used to train the event-based student encoder F jointly with a shared action decoder A , using a standard Behavior Cloning objective to predict the action of the teacher a_T . In parallel, we train an approximate student that receives state-based observations and aims to match the internal features h_S and action outputs a_S of the event-based student. Concretely, the approximate student is supervised using an L1 loss on the latent features of its encoder \hat{F}_S and the event-based student encoder F_S , and an MSE loss on the final action predictions, both computed using the shared action decoder A . This training process is depicted on the left side of Fig. 2.

To reduce the sim-to-real gap [47] in the event-based student encoder F_S , we incorporate the M3ED dataset [45] into the offline learning phase. This dataset includes event streams and depth maps collected from three platforms: a walking quadruped, a car, and a quadrotor. Since full state information is unavailable, and teacher actions cannot be queried, we introduce an auxiliary task that supervises the student encoder using depth-based labels. Specifically, the encoder is trained to predict 1-D angular distance maps, similar to a forward-facing single-line LiDAR scan restricted to the camera’s field of view, which resembles the perception input used by the teacher. For the teacher, these distance maps are horizontally aligned using the gravity vector to compensate for tilt. For the student, depth images are instead divided into three horizontal bands, and the minimum depth within 11.25° angular intervals is extracted for each band. The three resulting distance maps are then concatenated into a single 1-D observation. Using multiple bands reduces the need for gravity alignment by increasing the likelihood that at least one band captures an obstacle-free path, even when the pitch or roll causes other bands to face the ground or sky. These angular distance maps are predicted using a dedicated decoder D that processes the features from the event encoder. Similarly, using the rendered events in the offline dataset, the gravity-aligned distance maps that serve as input to the teacher are used to jointly train a separate auxiliary decoder D_o and the event encoder F_S , further infusing task-relevant information into the event feature space.

The offline learning stage alternates between two update steps: a Behavior Cloning and auxiliary depth task update using simulated event data, and an auxiliary depth task update using real-world data from the M3ED dataset. Specifically, each training iteration begins with a batch of real-world data used to update the event-based student encoder F_S and the dedicated distance decoder D responsible for predicting angular distance maps. This is followed by a batch from the simulated dataset, used to update the event-based student encoder F_S , the shared action decoder A , the approximate student \hat{F}_S , and the auxiliary decoder D_o . Through this alternating update scheme, the learned representation is both grounded in real-world event data and optimized for task relevance via supervision from expert demonstrations.

2) *Online Training*: To improve the generalization of the policy learned during offline training with BC, we further fine-tune the shared action decoder A through online interactions in simulation. Crucially, to avoid the computational cost of rendering event representations, we leverage the approximate student, which predicts the behavior of the event-based student using state observations. We adopt a classical DAgger framework [48], where both the teacher and the approximate student receive the same observations. An adaptive action sampling strategy, based on the difference between their predicted actions, gradually increases the proportion of actions taken by the student. This setup enables the collection of diverse experiences for training the action decoder A across a broader state distribution, while entirely bypassing the need for rendering events during online learning.

To prevent the action decoder A from learning two distinct manifolds for event–state alignment and state-based behavior fine-tuning, we add an offline alignment update in which the action decoder is supervised by predicting the teacher actions in the offline dataset using features from the event-based and approximate student. This offline update step adds minimal overhead, since the event features h_S for the offline data can be pre-computed once and reused for all fine-tuning runs.

3) *Network Architecture*: Our framework employs three networks: a teacher, an event-based student, and an approximate student. The teacher is implemented as a three-layer multilayer perceptron (MLP) with ReLU activations and a final tanh layer, following standard designs used in quadrotor control [14]. To efficiently process event representations and capture temporal dynamics, the event-based student uses an EfficientNet-B0 encoder [49], without the final classification layer, with two recurrent GRU layers inserted after the third and fourth stages of the backbone. The encoded spatial features are flattened through global average pooling and subsequently passed through the *Projection Layers*, which are implemented as a two-layer MLP with ReLU activations. The encoder of the approximate student is a lightweight three-layer MLP with ReLU activations. Both students share the same action decoder, which employs a fully connected *Fusion Layer* to merge the event features $h_s^{t_i}$ with the features produced by the *Vector Layers* from auxiliary inputs, namely the direction command $\vec{v}_{\text{cmd}}^{t_i}$, the previous action $a_S^{t_i-1}$, and, optionally, the quadrotor state s_{t_i} . The fused features are then further processed by a two-layer *Action Head* with ReLU activations and a final tanh layer. The processing pipeline of the event student is shown in Fig. 3. Both auxiliary decoders, D and D_o , are implemented as four-layer MLPs with ReLU activations. All networks are trained using the Adam optimizer [50], with a learning rate scheduled via cosine annealing with warm restarts [51]. The input to the event-based student consists of event representations with a resolution of 213×160 , obtained by downsampling the coordinates of an event stream originally at 640×480 . Importantly, this integer-division downsampling preserves certain high-resolution spatial details that would not be captured by a native 213×160 event camera, which requires the original event representations to be rendered at 640×480 .

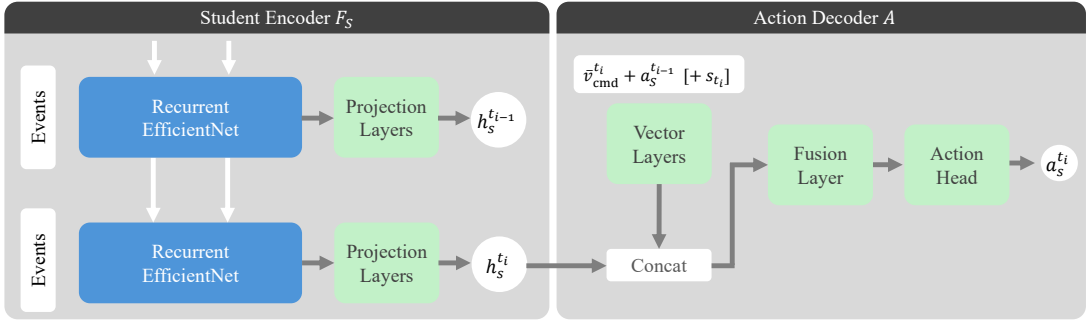


Fig. 3. **Event Student Overview.** The event representations are first encoded into features $h_S^{t_i}$ by the event student encoder F_S , which consists of a recurrent EfficientNet [49] followed by the *Projection Layers*. These event features are then concatenated with the outputs of the *Vector Layers*, which encode auxiliary inputs, i.e., the direction command \bar{v}_{t_i} , the previous action $a_S^{t_{i-1}}$, and, optionally, the state information s_{t_i} . The combined features are fused in the *Fusion Layer*, and the final actions $a_S^{t_i}$ are produced by the *Action Head*.

C. Event Rendering

Training end-to-end robot policies with visual inputs in simulation requires a large number of environment steps, which is particularly problematic for event-based policies because training time scales with the cost of simulating events. This cost is high, as accurate event simulation requires rendering high-frame-rate videos that capture the fine temporal resolution needed to truthfully simulate event sequences.

Each event sequence consists of individual events represented as tuples (\mathbf{x}_k, p_k, t_k) , where \mathbf{x}_k is the pixel location, $p_k \in \{+1, -1\}$ is the polarity, and t_k the timestamp. To simulate events, the event generation model in the noise-free scenario [4] is commonly used. Specifically, once a high-frame-rate video is synthesized, events are generated by evaluating the change in logarithmic intensity $L = \log(I_t)$ at a single pixel \mathbf{x}_k over time. An event is triggered at timestep t_k if the logarithmic intensity change from the last triggered event at timestep t_{k-1} exceeds a given contrast threshold C , as shown in Eq. 1.

$$\Delta L(\mathbf{x}_k, t_k) = L(\mathbf{x}_k, t_{k-1}) - L(\mathbf{x}_k, t_k) = p_k C. \quad (1)$$

Here, the polarity p_k indicates the direction of the intensity change. In popular video-to-event methods [52], [53], the frame rate of the underlying video is chosen such that the maximum optical flow between two frames does not exceed one pixel.

In our use case, the event stream is ultimately converted into a dense spatiotemporal representation, which is then processed by a lightweight neural network. Thus, generating a full event sequence only to later transform it into a dense representation introduces significant and unnecessary computational overhead. Inspired by [8], we follow the idea of directly generating event representations, effectively bypassing the intermediate step of synthesizing sparse event sequences. This design has two main advantages: (i) the direct generation of event representations reduces computation time and memory usage by avoiding explicit event sequence simulation, and (ii) it removes the need for high temporal fidelity, as the event representation uses a coarse discretization of the time dimension. In contrast to [8], which generates single-channel representations, our proposed approach truthfully constructs

Algorithm 1 Vectorized Event Representation Generation

Input Log frames $\{L_0, L_1, \dots, L_T\}$, contrast C

Output Event representation E_T

- 1: $\Delta L \leftarrow \{L_t - L_0 \mid t = 0, \dots, T\}$
- 2: $\text{BandID} \leftarrow \lfloor \Delta L / C \rfloor$
- 3: $\Delta \text{BandID} \leftarrow \text{BandID}_{1:T} - \text{BandID}_{0:T-1}$
- 4: $\text{FilteredBandID} \leftarrow \text{NonZero}(\Delta \text{BandID})$
- 5: $\Delta^2 \text{BandID} \leftarrow \text{FilteredBandID}_{1:F} - \text{FilteredBandID}_{0:F-1}$
- 6: $E_T \leftarrow \sum_{\text{axis}} [\Delta^2 \text{BandID} = 0]$

a multi-channel event tensor that accumulates the events in a given temporal window for each polarity [54]. Importantly, our method generates event representations for multiple videos in parallel using vectorized operations, significantly accelerating the simulation.

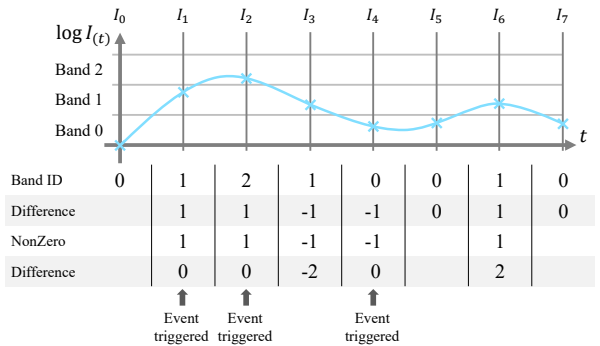


Fig. 4. **Vectorized Event Representation Generation.** Log intensities are quantized into bands, and band differences between adjacent timesteps are computed. Neighbouring non-zero values are then differenced again. Events are triggered where this second subtraction yields zero.

The core idea behind our event representation method is to leverage fast, vectorized operations, as illustrated in Fig. 4, which shows the log-intensity curve over time alongside the key processing steps. Given a high-frame-rate video with images I_0, I_1, \dots, I_7 , we first compute the log-intensity for each frame and subtract the intensity of the initial frame I_0 , establishing it as the reference. In the next step, each normalized log-intensity frame is floor-divided by the contrast threshold C , assigning each pixel at each timestep to a discrete

contrast band based on its current intensity level. To detect band transitions, we compute the temporal difference of band indices between consecutive frames. Steps where the band index remains unchanged, i.e., the difference equals zero, indicate no threshold crossing and are discarded. Crucially, an event is only triggered when the intensity curve exits the current band in the opposite direction from which it previously entered. To identify this, we compute a second-order difference of the band indices over time, using only frames with valid, non-zero first-order differences. An event is triggered at timesteps where this second difference is zero, indicating that the logarithmic difference exceeded the contrast threshold C . To obtain the final event representation, a simple reshaping and summing along a given axis is required. The event generation steps are summarized in Alg. 1.

To account for multiple events being triggered at a given pixel within a single timestep, we take the absolute value of the band ID difference in the first differencing step, which corresponds to the number of threshold crossings. Additionally, to simulate a non-zero initial reference value, a constant offset can be subtracted from the log-intensity at the normalization stage, allowing for flexible initialization of the reference state.

Our proposed event generation method enables the parallel generation of event representations for multiple video streams through efficient vectorized operations implemented in PyTorch [55]. Except for a few corner cases related to specific initial conditions, the resulting event representations are numerically equivalent to those obtained by first generating full event sequences with ESIM [53] and subsequently converting them to dense representations. While our approach reduces average runtime by 34% compared to generating event representations with ESIM’s CUDA-based implementation, its primary advantage lies in the significantly improved memory efficiency, illustrated in Fig. 5. Compared to ESIM, our method substantially reduces the maximum GPU memory usage, which ultimately determines whether event simulations at scale are feasible. Consequently, ESIM fails to scale to higher resolutions and larger numbers of environments, restricting the comparison in Fig. 5 to half the final resolution (240×320) and at most 15 environments. In contrast, our method supports large-scale parallel simulation environments, making it well-suited for training event-based control policies at scale.

D. Teacher Training

The teacher policy is trained using Proximal Policy Optimization (PPO) [56] within the Flightmare simulator [44]. Its observation space includes the commanded direction in the local frame, the z-position of the quadrotor, orientation represented as a flattened rotation matrix, linear and angular velocities, and the previous action command. To perceive obstacles, the teacher also receives an angular distance map that encodes the closest obstacle distances across 10 angular bins. Each bin spans 11.25° , covering a 120-degree horizontal field of view. The episode terminates if the quadrotor leaves the simulation boundary, collides with an obstacle, or reaches the maximum number of steps. The teacher is trained for 8000 PPO update steps, with each update performed on rollouts of 250 steps collected from 100 parallel environments.

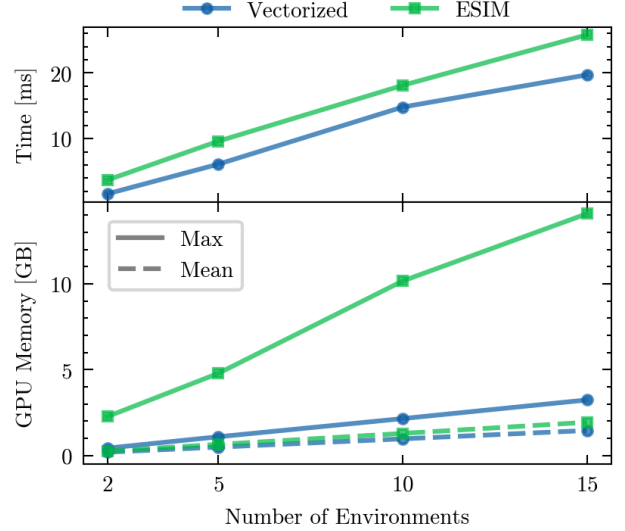


Fig. 5. **Runtime and Memory Requirements.** The maximum and mean GPU memory usage and the required computation time are shown for our vectorized event generation (Vectorized) and ESIM’s GPU-based event generation (ESIM) across different numbers of environments. Our method leads to a 34% reduction in mean runtime (top) and significantly lowers peak GPU memory usage (bottom).

The total reward r_t combines several weighted components, with their respective factors λ_* omitted in Eq. 2 for clarity:

$$r_t = r_{\text{prog}} + r_{\text{act}} + r_{\text{br}} + r_{\text{perc}} + r_{\text{obs_dist}} + r_{\text{crash}} \quad (2)$$

$$\begin{aligned}
 r_{\text{prog}} &= \tanh\left(\frac{\bar{v}_{\text{quad}} \cdot \bar{v}_{\text{cmd}}}{\|\bar{v}_{\text{cmd}}\|} + 1\right) \\
 &\quad \cdot \tanh\left(\|\bar{v}_{\text{cmd}}\| - \|\bar{v}_{\text{quad}} - \bar{v}_{\text{cmd}}\| + 1\right) \\
 &\quad \cdot \frac{1}{4} \min\left(\frac{\|\bar{v}_{\text{quad}}\|}{\|\bar{v}_{\text{cmd}}\|}, 1\right) - |v_{\text{quad}}^z|, \\
 r_{\text{act}} &= -\|\bar{a}_{t_i} - \bar{a}_{t_{i-1}}\|, \\
 r_{\text{br}} &= -\|\bar{a}_\omega\|, \\
 r_{\text{perc}} &= \frac{\bar{v}_{\text{cmd}} \cdot \bar{d}_{\text{heading}}}{\|\bar{v}_{\text{cmd}}\| \|\bar{d}_{\text{heading}}\|}, \\
 r_{\text{obs_dist}} &= -\frac{1}{N_{\text{obs}}} \sum_i^{N_{\text{obs}}} \exp(-d_{\text{obs}_i} - (\phi_{\text{heading}} - \beta_{\text{obs}_i})^2) \\
 r_{\text{crash}} &= -\|\bar{v}_{\text{quad}}\| - 1 \quad \text{if crash ceiling, ground or obstacle,}
 \end{aligned} \quad (3)$$

where r_{prog} encourages the quadrotor velocity \bar{v}_{quad} to align with the commanded direction \bar{v}_{cmd} to promote goal-directed flight, r_{act} penalizes large changes in consecutive actions \bar{a}_{t_i} to ensure smooth control, r_{br} discourages high body-rate actions \bar{a}_ω to support stable flight dynamics, r_{perc} rewards alignment of the yaw direction of the quadrotor \bar{d}_{heading} with the commanded direction, $r_{\text{obs_dist}}$ exponentially penalizes the distance d_{obs_i} to nearby obstacles N_{obs} inside the field of view $(\phi_{\text{heading}} - \beta_{\text{obs}_i})$, and r_{crash} applies a penalty upon collisions or when the quadrotor exits the simulation boundaries. Overall, the proposed teacher formulation yields a stable state-based policy capable of reliably flying in highly cluttered environments.

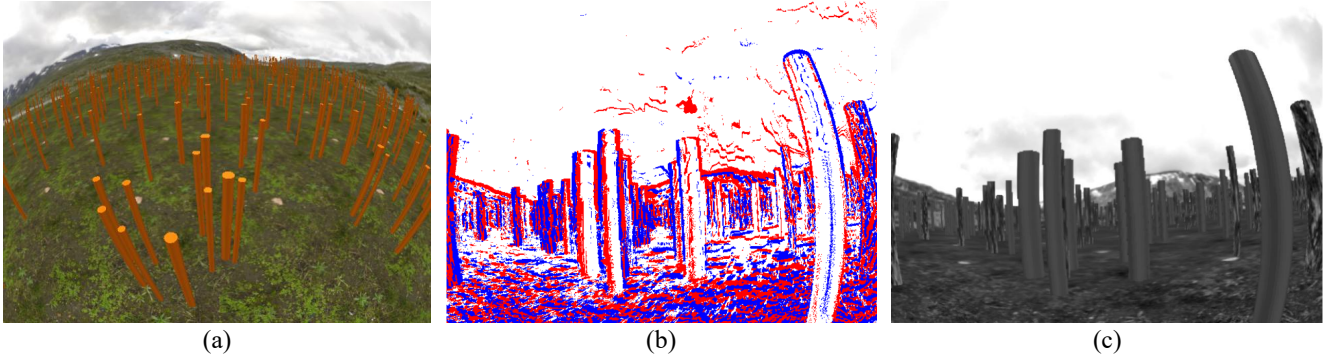


Fig. 6. **Simulation Environment.** The environment consists of tall cylindrical obstacles placed in a natural scene (a). The scene is captured by a simulated event camera mounted on the quadrotor (b). For reference, the corresponding grayscale images are also shown (c).

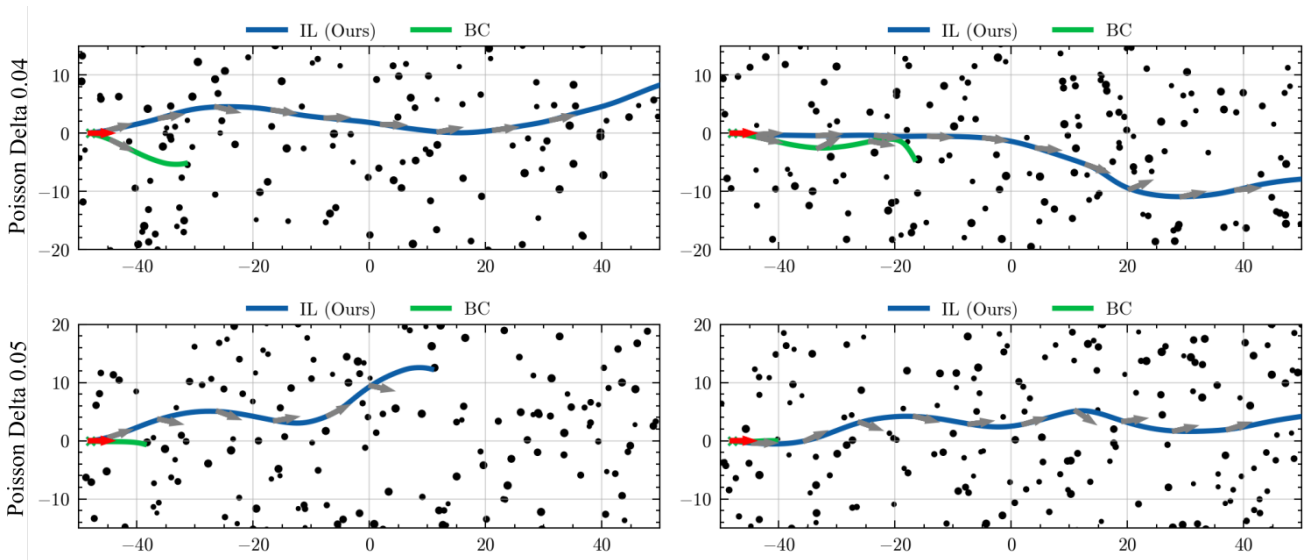


Fig. 7. **Top-down View of Flight Trajectories in Simulation.** Our proposed method yields a policy that consistently flies longer trajectories than BC, the closest baseline applicable in the same training setting.

IV. EXPERIMENTS

To evaluate our proposed algorithm, we conduct experiments in simulation using Flightmare [44], as described in Sec. IV-A, and validate its performance in the real world using a quadrotor setup similar to [43], detailed in Sec. IV-B.

A. Simulation

1) *Setup:* To validate our approach, we construct a simulated forest environment where trees are modeled as tall cylinders with radii ranging from 0.2 m to 0.5 m. These cylinders are placed within a $100\text{ m} \times 100\text{ m}$ world box rendered in a natural outdoor scene (Fig. 6). Tree positions are sampled using a Poisson point process, with the Poisson delta varied to control the tree density across different environments. For each Poisson delta value (0.04 and 0.05), we sample 10 environments, resulting in 20 distinct test environments. In each test episode, the quadrotor starts at the center of the left edge of the environment and receives a direction command pointing toward the right side. We consider a flight successful if the quadrotor travels more than 40 m in the commanded

direction without crashing into the obstacles or leaving the world box.

2) *Results:* As shown in Tab. II, our approach outperforms Behavior Cloning (BC) and DAgger [48], and matches the performance of the combined BC+DAgger baseline, despite the latter relying on online event renderings and requiring a substantially longer training time. Our method achieves a success rate that is 0.2 higher than BC (1.0 vs. 0.8), since BC does not benefit from our proposed behavior fine-tuning via lightweight simulation, as illustrated by the example test flights in Fig. 7. When increasing the tree density to a Poisson delta of 0.05, the performance of our approach decreases from 1.00 to 0.80, while still maintaining a 0.20 advantage compared to BC. Despite having access to online event rendering, the number of rendering steps used for our approach is insufficient for DAgger to learn a robust mapping from events and state information to control commands. Moreover, the equal performance of our approximate IL and the BC+DAgger baseline demonstrates that our approximation with lightweight states is sufficiently close to real event renderings, while substantially reducing the behavior training time, as illustrated in Fig. 13.

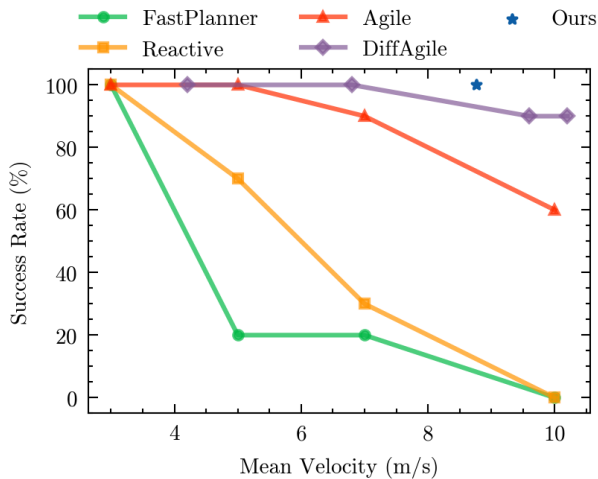


Fig. 8. **Representative Comparison.** This illustrative comparison places our method in context by showing the achieved mean velocity and success rates reported by baseline methods, which benefit from having absolute depth information as input.

TABLE I
SIMULATION RESULTS WITHOUT QUADROTOR STATE.

Methods	Poisson Delta: 0.04	
	Success Rate	Mean Velocity [$\frac{m}{s}$]
BC	0.20	8.08
Approx IL (Ours)	0.50	8.17

Finally, our event student achieves a comparable performance to the teacher that relies on highly informative distance maps, confirming that the teacher–student performance gap is small.

The advantage of our proposed approximate IL method over BC, which represents the best-performing baseline applicable in the same training conditions, also becomes evident in a more constrained setting where only onboard inputs are available, namely, the previous actions and the commanded direction. Without access to the quadrotor state, our method improves the success rate by 0.3 compared to BC (0.5 vs. 0.2), as reported in Tab. I. Crucially, both approaches rely on the same number of pre-rendered event representations, since our method avoids costly online event rendering by leveraging approximate policy updates in simulation. The BC baseline can thus be interpreted as an ablation of our approach without the proposed online fine-tuning using lightweight state information.

3) *Ablations:* To validate our design choices, we conduct several ablation studies in simulation using the standard model, i.e., the event-based policy with access to state information. The evaluation environments are generated with a Poisson delta of 0.04. Our first ablation examines which components of the network should remain trainable during approximate IL, as summarized in Tab. III. In the default configuration, we fine-tune the *Vector Encoder* and the *Fusion Layer*, which leads to the longest mean flight distance before a crash. When all parameters of the action decoder are updated (Full Action Decoder), the policy still reaches 94.1 m and maintains a high speed of 9.14 m s^{-1} . Reducing further the number of trainable parameters, either by updating only the biases (Only Biases) or

by updating only the final layer (Last Layer), results in slower flight speeds and significantly shorter flight distances, e.g., 46.67 m when updating only the last layer. This degradation can be explained by the reduced adaptability of the policy that results from limiting the set of trainable parameters. Overall, the best performance is achieved when updating the *Vector Encoder* and the *Fusion Layer*, which suggests that there is an optimal trade-off between adapting the policy during the approximate IL phase and preserving the knowledge learned during the pretraining stage.

To assess the effect of the quadrotor state observations, we ablate policies that receive varying levels of state information, as reported in Tab. IV. Naturally, providing full state information leads to the highest robustness with a success rate of 1.0. The removal of angular velocities (w/o Angular Vel.) has little impact, as the resulting policy still achieves a perfect success rate. In contrast, excluding translational velocities (w/o Transl. Vel.) reduces the success rate to 0.8 while increasing the mean flight speed to 12.91 m s^{-1} , reflecting the difficulty in controlling the speed without absolute velocity observations. The differing impact of removing angular versus translational velocities can be explained by the ability of the event camera to infer rotational motion through its high temporal resolution, whereas the absolute scale information required to estimate translational velocity is inherently missing in monocular sensing. When both angular and translational velocities are removed (w/o Vel.), the success rate drops further to 0.7, approaching the performance obtained without any state information (w/o State), which reaches 0.5.

4) *Representative Comparison:* To put the performance of our method into context with existing work, we plot the results reported in related work [5] in Fig. 8 and include the performance of our method for reference. Although the forest density and evaluation metrics are the same across methods, the underlying simulators and environments differ. Furthermore, the reported baselines FastPlanner [57], Reactive [58], Agile [43], and DiffAgile [5] use depth information in addition to state information. This represents a significant advantage over our monocular setup, which must infer depth from a single event camera. Consequently, this comparison should be interpreted as a representative reference to relate the different success rates and achieved velocities, rather than as a direct one-to-one comparison.

B. Real-World

1) *Hardware Setup:* We validate our approach in the real world using a quadrotor platform and onboard computational resources similar to those used in [43]. The quadrotor is equipped with Hobbywing XRotor 2306 motors and 5-inch propellers, resulting in a total weight of approximately 780 g. Onboard computation is handled by an NVIDIA Jetson TX2, mounted on a ConnectTech Quasar carrier board. Our neural network outputs control commands in the form of collective thrust and angular rates, which are converted to individual rotor commands using the BetaFlight flight controller. For event-based perception, we use the DVXplorer Micro sensor with a VGA resolution of 640×480 pixels, weighing approximately

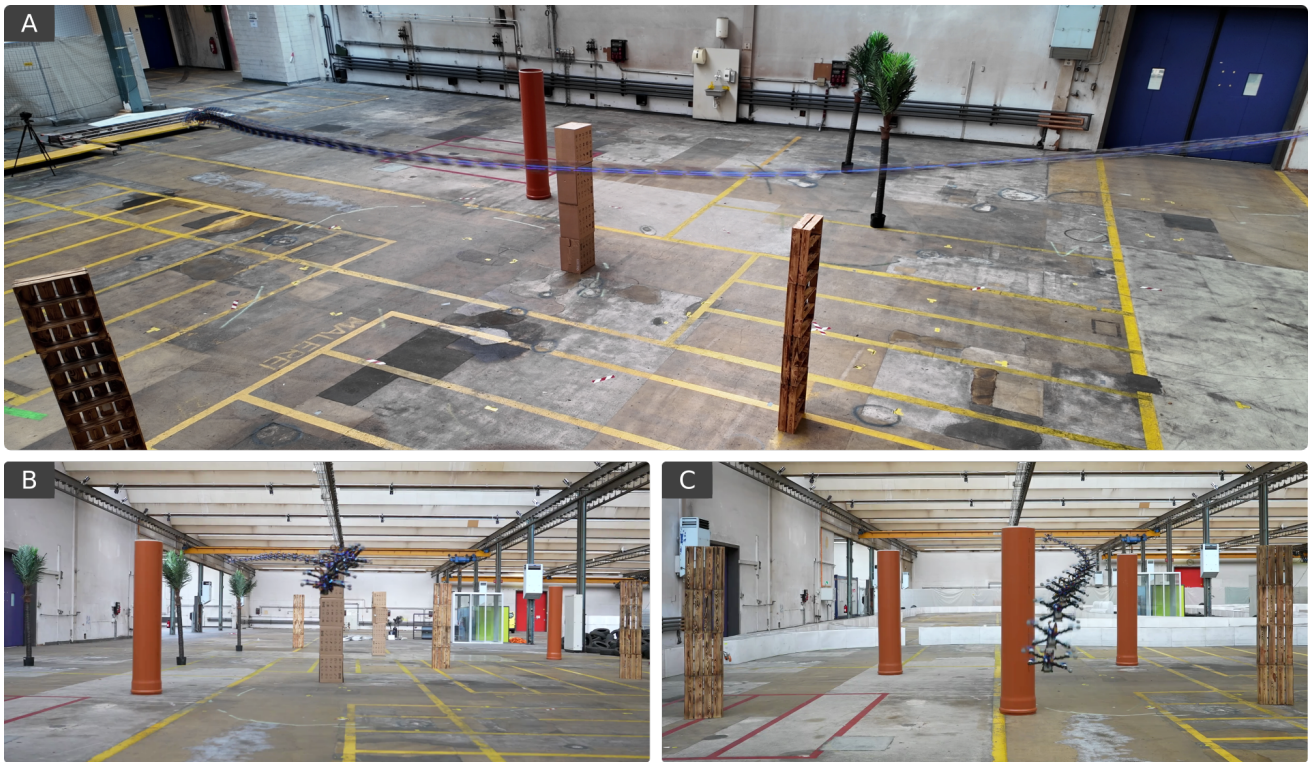


Fig. 9. **Real-World Flights.** Our end-to-end policy demonstrates reliable flight in complex (A/B) and moderately cluttered (C) real-world environments using only a monocular event camera and onboard compute.

TABLE II
SIMULATION RESULTS IN ENVIRONMENTS WITH VARYING OBSTACLE DENSITIES PARAMETERIZED BY THE POISSON DELTA.

Methods	Training Input	Poisson Delta: 0.04		Poisson Delta: 0.05	
		Success Rate	Mean Velocity [$\frac{m}{s}$]	Success Rate	Mean Velocity [$\frac{m}{s}$]
BC	Offline Event	0.80	8.53	0.70	8.13
Dagger [48]	Online Event	0.30	6.66	0.10	5.72
BC+Dagger	Offline Event + Online Event	1.00	9.00	0.90	8.47
Approx IL (Ours)	Offline Event + Online State	1.00	8.76	0.90	8.53
State Teacher (Ours)	Online State + Dist. Map	1.00	8.77	0.90	8.60

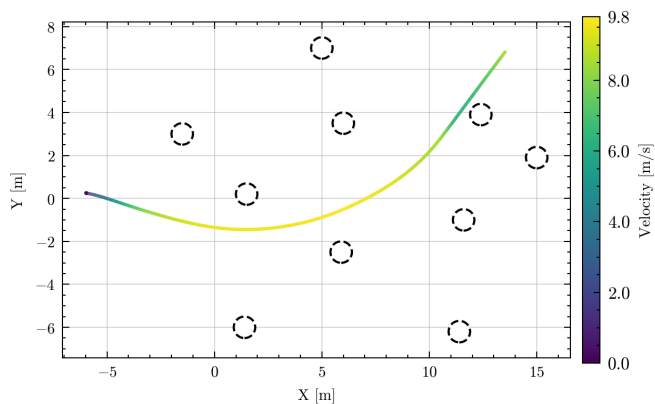


Fig. 10. **Top-down View of a Real-World Flight Trajectory.** The velocity of the quadrotor at each timestep is visualized using the color mapping on the right, reaching up to 9.8 m s^{-1} , alongside the approximate obstacle locations.

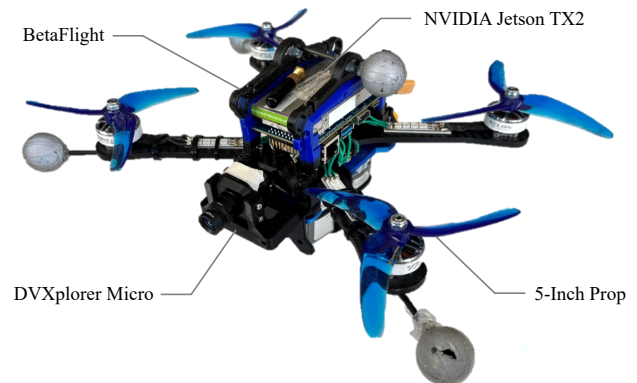


Fig. 11. **Quadrotor Platform.** The platform used in the real-world experiments features an NVIDIA Jetson TX2 running the event-based student, which processes events from a DVXplorer Micro sensor.

16 g without a lens. Although the DVXplorer Micro includes an onboard IMU, we do not use its inertial measurements

in our approach. Using TensorRT, a forward pass of our event network processing 213×160 event representations takes

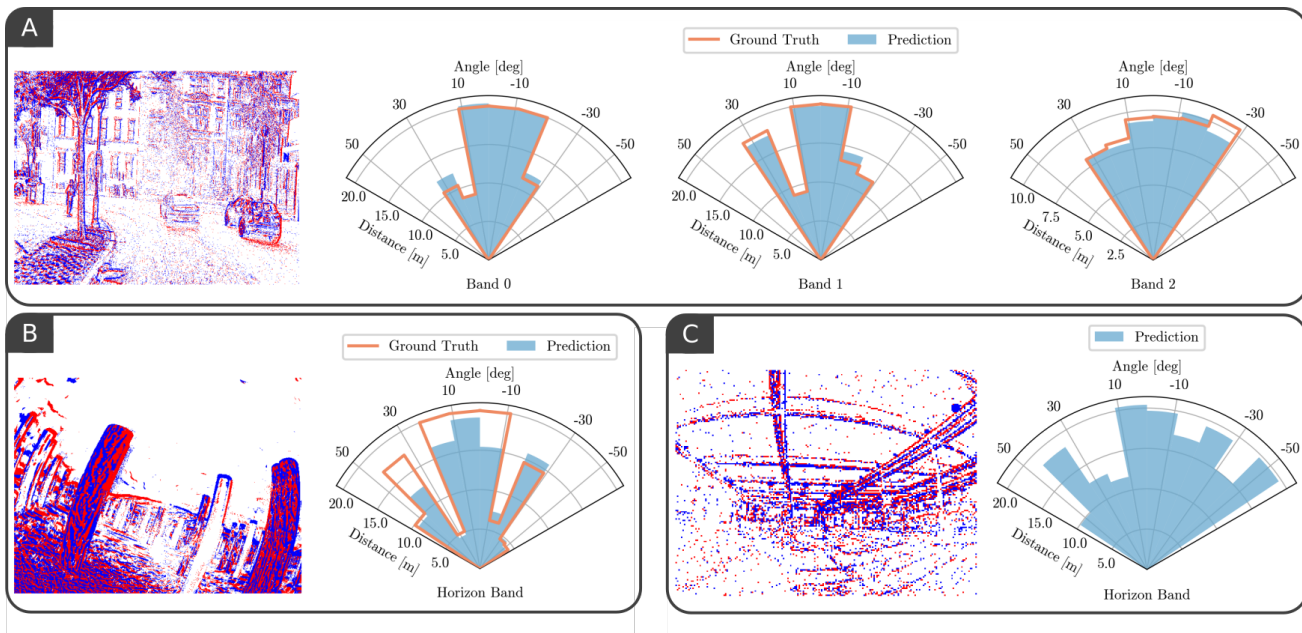


Fig. 12. **Distance Map Estimation** The ground truth distance maps and corresponding predictions are shown for the M3ED dataset (A), simulation data (B), and the real-world test environment (C). Importantly, the distance maps and associated auxiliary decoders are used only during pretraining and are not involved in action inference of the event student.

TABLE III
ABLATION OF TRAINABLE ACTION DECODER PARAMETERS.

Methods	Mean Distance [m]	Mean Velocity [$\frac{m}{s}$]
Only Biases	76.60	7.76
Last Layer	46.67	8.44
Full Action Decoder	94.10	9.14
Vector+Fusion (Default)	110.3	8.76

TABLE IV
ABLATION OF VARYING STATE INFORMATION LEVELS.

Methods	Success Rate	Mean Velocity [$\frac{m}{s}$]
w/o State	0.50	8.17
w/o Vel.	0.70	11.55
w/o Transl. Vel.	0.80	12.91
w/o Angular Vel.	1.00	9.04
w State	1.00	8.76

on average 11.6 ms on the Jetson TX2, providing sufficient margin to meet the 20 ms requirement of the 50 Hz control frequency.

2) *Results*: Our event-based policy is capable of flying reliably through indoor environments with varying levels of clutter using quadrotor state estimates from an external positioning system, as shown in Fig. 9. Tested in five environments with obstacle counts that increase from sparse to dense, reaching up to ten obstacles, the quadrotor equipped with a single event camera successfully navigates trajectories through the cylindrical obstacles. The policy reaches velocities of up to 9.8 m s^{-1} in these indoor tests, as illustrated in Fig. 10, which shows the velocity profile along the trajectory together with the approximate obstacle locations. This strong performance achieved by an end-to-end event policy is likely supported by the inclusion of real-world event data during the pretraining

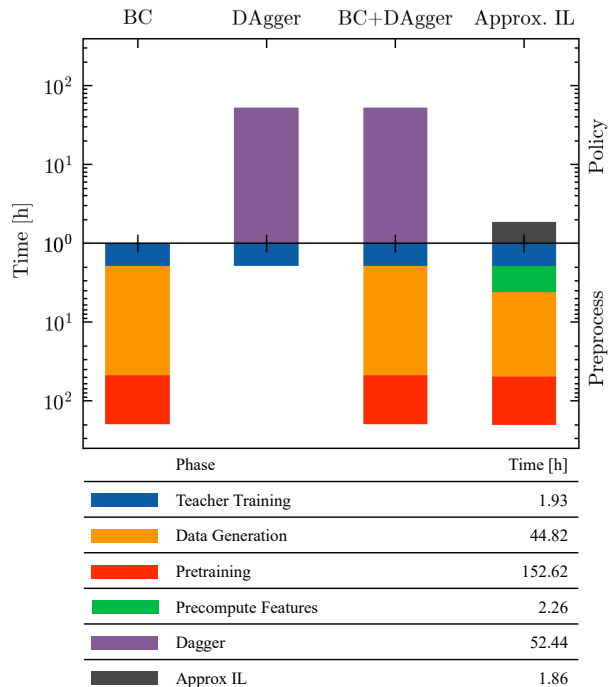


Fig. 13. **Training Time**. Comparison of the time required by each baseline for the individual training steps, grouped into a *Preprocess* and a *Policy* stage.

stage of our approximate IL framework, which helps facilitate transfer from simulation to the real world.

C. Training Time

In Fig. 13, we report the time required by each baseline for the individual training steps, grouped into a *Preprocess*

stage and a *Policy* stage. The *Preprocess* stage consists of steps that can typically be reused across multiple policy trainings and therefore do not significantly contribute to the time needed to develop a new policy. In contrast, the *Policy* stage includes steps that must be executed for every new policy. Since all evaluated methods operate within an Imitation Learning framework, each method requires training a teacher policy using lightweight state and perception observations, which is computationally inexpensive and takes 1.93 h. Except for DAgger, all methods also require 44.82 h to generate offline data, including event renderings (Data Generation) and 152.62 h for the subsequent training on this offline dataset (Pretraining). To reduce training time in the *Policy* stage, our proposed Approx. IL precomputes event features in 2.26 h for all samples in the offline dataset, which is possible because its event encoder remains frozen during policy fine-tuning. The substantial improvement provided by Approx. IL becomes evident in the *Policy* stage, where the reliance of DAgger methods on online event rendering leads to a training time of 52.44 h, whereas Approx. IL requires only 1.86 h. This corresponds to a reduction in training time by approximately a factor of 28.

D. Distance Map Estimation

To provide insight into the angular distance map estimation, we visualize sample predictions alongside the corresponding ground truth in Fig. 12. Importantly, the distance maps and associated auxiliary decoders D and D_o are used only during the pretraining phase and are discarded during action inference of the event student. In Fig. 12 (A), we show the three ground truth distance bands together with the corresponding predictions for the M3ED dataset, as described in Sec. III-B1. Even though this sample comes from a hold-out validation split, the auxiliary decoder D accurately predicts the angularly binned distances in an automotive scene. On simulation data, the auxiliary decoder D_o reliably predicts gravity-aligned angular distance maps, as illustrated in Fig. 12 (B). Finally, Fig. 12 (C) shows a prediction of a gravity-aligned angular distance map in the real-world test environment onboard a hovering quadrotor. These qualitative examples demonstrate that the auxiliary decoders can robustly predict angular distance maps using only events, providing evidence that the feature space of the event encoder captures meaningful distance information.

V. CONCLUSION

While event cameras offer compelling advantages such as high temporal resolution and low latency, their adoption in real-world robotics has been limited by the high computational cost of simulating events for policy learning. In this work, we propose an approximate imitation learning framework that significantly reduces the number of required event renderings by leveraging offline datasets from both simulation and the real world. To increase the generalization of the policy behaviour, we introduce an approximate student that predicts the actions of the event-based student using privileged state information. Since this state information can be simulated efficiently, the policy can be fine-tuned through online interactions without

rendering events. To further accelerate validation of event-based policies in simulation, we also propose a fully parallelized method to directly generate event representations from high-speed videos. Experiments in both simulation and the real world demonstrate that our approach enables fast and agile quadrotor flight through cluttered environments using a single event camera, without relying on intermediate representations. While we apply our approximate IL to event data, the framework naturally extends to other modalities that are expensive to simulate, such as tactile sensors, radar, or LiDAR.

REFERENCES

- [1] C. Cadena, L. Carlone, H. Carrillo, Y. Latif, D. Scaramuzza, J. Neira, I. Reid, and J. J. Leonard, "Past, present, and future of simultaneous localization and mapping: Toward the robust-perception age," *IEEE Transactions on robotics*, vol. 32, no. 6, pp. 1309–1332, 2017.
- [2] S. Levine, C. Finn, T. Darrell, and P. Abbeel, "End-to-end training of deep visuomotor policies," *Journal of Machine Learning Research*, vol. 17, no. 39, pp. 1–40, 2016.
- [3] A. Kendall, J. Hawke, D. Janz, P. Mazur, D. Reda, J.-M. Allen, V.-D. Lam, A. Bewley, and A. Shah, "Learning to drive in a day," in *2019 international conference on robotics and automation (ICRA)*. IEEE, 2019, pp. 8248–8254.
- [4] G. Gallego, T. Delbruck, G. Orchard, C. Bartolozzi, B. Taba, A. Censi, S. Leutenegger, A. Davison, J. Conradt, K. Daniilidis, and D. Scaramuzza, "Event-based vision: A survey," *IEEE Trans. Pattern Anal. Mach. Intell.*, 2020.
- [5] Y. Zhang, Y. Hu, Y. Song, D. Zou, and W. Lin, "Learning vision-based agile flight via differentiable physics," *Nature Machine Intelligence*, vol. 7, no. 6, p. 954–966, Jun. 2025. [Online]. Available: <http://dx.doi.org/10.1038/s42256-025-01048-0>
- [6] Y. Ren, F. Zhu, G. Lu, Y. Cai, L. Yin, F. Kong, J. Lin, N. Chen, and F. Zhang, "Safety-assured high-speed navigation for mavs," *Science Robotics*, vol. 10, no. 98, p. ead06187, 2025.
- [7] D. Falanga, K. Kleber, and D. Scaramuzza, "Dynamic obstacle avoidance for quadrotors with event cameras," *Science Robotics*, vol. 5, no. 40, p. eaaz9712, 2020.
- [8] A. Bhattacharya, M. Cannici, N. Rao, Y. Tao, V. Kumar, N. Matni, and D. Scaramuzza, "Monocular event-based vision for obstacle avoidance with a quadrotor," in *8th Annual Conference on Robot Learning*, 2024.
- [9] S. Ross, G. Gordon, and D. Bagnell, "A reduction of imitation learning and structured prediction to no-regret online learning," in *Proceedings of the Fourteenth International Conference on Artificial Intelligence and Statistics*, ser. Proceedings of Machine Learning Research, G. Gordon, D. Dunson, and M. Dudík, Eds., vol. 15. Fort Lauderdale, FL, USA: PMLR, 11–13 Apr 2011, pp. 627–635.
- [10] T. Haarnoja, B. Moran, G. Lever, S. H. Huang, D. Tirumala, J. Humplik, M. Wulfmeier, S. Tunyasuvunakool, N. Y. Siegel, R. Hafner *et al.*, "Learning agile soccer skills for a bipedal robot with deep reinforcement learning," *Science Robotics*, vol. 9, no. 89, p. eadi8022, 2024.
- [11] J. Hwangbo, J. Lee, A. Dosovitskiy, D. Bellicoso, V. Tsounis, V. Koltun, and M. Hutter, "Learning agile and dynamic motor skills for legged robots," *Science Robotics*, vol. 4, no. 26, p. eaau5872, 2019.
- [12] O. M. Andrychowicz, B. Baker, M. Chociej, R. Jozefowicz, B. McGrew, J. Pachocki, A. Petron, M. Plappert, G. Powell, A. Ray *et al.*, "Learning dexterous in-hand manipulation," *The International Journal of Robotics Research*, vol. 39, no. 1, pp. 3–20, 2020.
- [13] E. Aljalbout, F. Frank, M. Karl, and P. van der Smagt, "On the role of the action space in robot manipulation learning and sim-to-real transfer," *IEEE Robotics and Automation Letters*, 2024.
- [14] J. Xing, I. Geles, Y. Song, E. Aljalbout, and D. Scaramuzza, "Multi-task reinforcement learning for quadrotors," *IEEE Robotics and Automation Letters*, 2024.
- [15] C. Chi, S. Feng, Y. Du, Z. Xu, E. Cousineau, B. Burchfiel, and S. Song, "Diffusion policy: Visuomotor policy learning via action diffusion," in *Proceedings of Robotics: Science and Systems (RSS)*, 2023.
- [16] D. Shah, A. Sridhar, N. Dashora, K. Stachowicz, K. Black, N. Hirose, and S. Levine, "ViNT: A foundation model for visual navigation," in *7th Annual Conference on Robot Learning*, 2023. [Online]. Available: <https://arxiv.org/abs/2306.14846>
- [17] Z. Fu, T. Z. Zhao, and C. Finn, "Mobile aloha: Learning bimanual mobile manipulation with low-cost whole-body teleoperation," in *Conference on Robot Learning (CoRL)*, 2024.

- [18] S. Nair, A. Rajeswaran, V. Kumar, C. Finn, and A. Gupta, “R3m: A universal visual representation for robot manipulation,” *arXiv preprint arXiv:2203.12601*, 2022.
- [19] Y. J. Ma, S. Sodhani, D. Jayaraman, O. Bastani, V. Kumar, and A. Zhang, “Vip: Towards universal visual reward and representation via value-implicit pre-training,” *arXiv preprint arXiv:2210.00030*, 2022.
- [20] J. Xing, L. Bauersfeld, Y. Song, C. Xing, and D. Scaramuzza, “Contrastive learning for enhancing robust scene transfer in vision-based agile flight,” in *2024 IEEE International Conference on Robotics and Automation (ICRA)*. IEEE, 2024, pp. 5330–5337.
- [21] S. Stroobants, J. Dupeyroux, and G. C. de Croon, “Neuromorphic computing for attitude estimation onboard quadrotors,” *Neuromorphic Computing and Engineering*, vol. 2, no. 3, p. 034005, 2022.
- [22] S. Stroobants, C. De Wagter, and G. C. De Croon, “Neuromorphic attitude estimation and control,” *IEEE Robotics and Automation Letters*, 2025.
- [23] F. Paredes-Vallés, J. J. Hagenaaers, J. Dupeyroux, S. Stroobants, Y. Xu, and G. de Croon, “Fully neuromorphic vision and control for autonomous drone flight,” *Science Robotics*, vol. 9, no. 90, p. eadi0591, 2024.
- [24] A. Vitale, A. Renner, C. Nauer, D. Scaramuzza, and Y. Sandamirskaya, “Event-driven vision and control for uavs on a neuromorphic chip,” in *2021 IEEE International Conference on Robotics and Automation (ICRA)*. IEEE, 2021, pp. 103–109.
- [25] K. F. Andersen, H. X. Pham, H. I. Ugurlu, and E. Kayacan, “Event-based navigation for autonomous drone racing with sparse gated recurrent network,” in *2022 European Control Conference (ECC)*. IEEE, 2022, pp. 1342–1348.
- [26] X. Zhang, J. Tie, J. Li, Y. Hu, S. Liu, X. Li, Z. Li, X. Yu, J. Zhao, Z. Wan *et al.*, “Dynamic obstacle avoidance for unmanned aerial vehicle using dynamic vision sensor,” in *International Conference on Artificial Neural Networks*. Springer, 2023, pp. 161–173.
- [27] K. Mohta, M. Watterson, Y. Mulgaonkar, S. Liu, C. Qu, A. Makineni, K. Saulnier, K. Sun, A. Zhu, J. Delmerico *et al.*, “Fast, autonomous flight in gps-denied and cluttered environments,” *Journal of Field Robotics*, vol. 35, no. 1, pp. 101–120, 2018.
- [28] M. Tranzatto, T. Miki, M. Dharmadhikari, L. Bernreiter, M. Kulkarni, F. Mascarich, O. Andersson, S. Khattak, M. Hutter, R. Siegwart *et al.*, “Cerberus in the darpa subterranean challenge,” *Science Robotics*, vol. 7, no. 66, p. eabp9742, 2022.
- [29] M. Bloesch, S. Omari, M. Hutter, and R. Siegwart, “Robust visual inertial odometry using a direct ekf-based approach,” in *2015 IEEE/RSJ international conference on intelligent robots and systems (IROS)*. IEEE, 2015, pp. 298–304.
- [30] C. Forster, Z. Zhang, M. Gassner, M. Werlberger, and D. Scaramuzza, “Svo: Semidirect visual odometry for monocular and multicamera systems,” *IEEE Transactions on Robotics*, vol. 33, no. 2, pp. 249–265, 2016.
- [31] S. Karaman and E. Frazzoli, “Incremental sampling-based algorithms for optimal motion planning,” *Robotics Science and Systems VI*, vol. 104, no. 2, pp. 267–274, 2010.
- [32] A. Bircher, M. Kamel, K. Alexis, H. Oleynikova, and R. Siegwart, “Receding horizon” next-best-view” planner for 3d exploration,” in *2016 IEEE international conference on robotics and automation (ICRA)*. IEEE, 2016, pp. 1462–1468.
- [33] F. Sadeghi and S. Levine, “Cad2rl: Real single-image flight without a single real image,” *Robotics: Science and Systems*, 2016.
- [34] E. Kaufmann, A. Loquercio, R. Ranftl, A. Dosovitskiy, V. Koltun, and D. Scaramuzza, “Deep drone racing: Learning agile flight in dynamic environments,” in *Proceedings of The 2nd Conference on Robot Learning*, ser. Proceedings of Machine Learning Research, A. Billard, A. Dragan, J. Peters, and J. Morimoto, Eds., vol. 87. PMLR, 29–31 Oct 2018, pp. 133–145.
- [35] A. Loquercio, A. I. Maqueda, C. R. Del-Blanco, and D. Scaramuzza, “Dronet: Learning to fly by driving,” *IEEE Robotics and Automation Letters*, vol. 3, no. 2, pp. 1088–1095, 2018.
- [36] D. Shah, A. Sridhar, A. Bhorkar, N. Hirose, and S. Levine, “GNM: A General Navigation Model to Drive Any Robot,” in *International Conference on Robotics and Automation (ICRA)*, 2023. [Online]. Available: <https://arxiv.org/abs/2210.03370>
- [37] A. Sridhar, D. Shah, C. Glossop, and S. Levine, “NoMaD: Goal Masked Diffusion Policies for Navigation and Exploration,” *arXiv pre-print*, 2023. [Online]. Available: <https://arxiv.org/abs/2310.07896>
- [38] E. Kaufmann, L. Bauersfeld, A. Loquercio, M. Müller, V. Koltun, and D. Scaramuzza, “Champion-level drone racing using deep reinforcement learning,” *Nature*, vol. 620, no. 7976, pp. 982–987, 2023.
- [39] I. Geles, L. Bauersfeld, A. Romero, J. Xing, and D. Scaramuzza, “Demonstrating agile flight from pixels without state estimation,” *Robotics: Science and Systems (RSS)*, 2024.
- [40] J. Xing, A. Romero, L. Bauersfeld, and D. Scaramuzza, “Bootstrapping reinforcement learning with imitation for vision-based agile flight,” *8th Conference on Robot Learning (CoRL)*, 2024.
- [41] A. Romero, A. Shenai, I. Geles, E. Aljalbout, and D. Scaramuzza, “Dream to fly: Model-based reinforcement learning for vision-based drone flight,” *arXiv preprint arXiv:2501.14377*, 2025.
- [42] F. Torabi, G. Warnell, and P. Stone, “Behavioral cloning from observation,” in *IJCAI*, 2018, pp. 4950–4957.
- [43] A. Loquercio, E. Kaufmann, R. Ranftl, M. Müller, V. Koltun, and D. Scaramuzza, “Learning high-speed flight in the wild,” in *Science Robotics*, October 2021.
- [44] Y. Song, S. Naji, E. Kaufmann, A. Loquercio, and D. Scaramuzza, “Flightmare: A flexible quadrotor simulator,” in *Proceedings of the 2020 Conference on Robot Learning*, 2021, pp. 1147–1157.
- [45] K. Chaney, F. Cladera, Z. Wang, A. Bisulco, M. A. Hsieh, C. Korpela, V. Kumar, C. J. Taylor, and K. Daniilidis, “M3ed: Multi-robot, multi-sensor, multi-environment event dataset,” in *Proceedings of the IEEE/CVF Conference on Computer Vision and Pattern Recognition (CVPR) Workshops*, June 2023, pp. 4015–4022.
- [46] N. Messikommer, J. Xing, E. Aljalbout, and D. Scaramuzza, “Student-informed teacher training,” *International Conference on Learning Representations*, 2025.
- [47] E. Aljalbout, J. Xing, A. Romero, I. Akinola, C. Garrett, E. Heiden, A. Gupta, T. Hermans, Y. Narang, D. Fox, D. Scaramuzza, and F. Ramos, “The reality gap in robotics: Challenges, solutions, and best practices,” *arXiv preprint*, 2025.
- [48] S. Ross, G. Gordon, and D. Bagnell, “A reduction of imitation learning and structured prediction to no-regret online learning,” in *Proceedings of the fourteenth international conference on artificial intelligence and statistics. JMLR Workshop and Conference Proceedings*, 2011, pp. 627–635.
- [49] M. Tan and Q. Le, “Efficientnet: Rethinking model scaling for convolutional neural networks,” in *International conference on machine learning*. PMLR, 2019, pp. 6105–6114.
- [50] D. P. Kingma and J. L. Ba, “Adam: A method for stochastic optimization,” *Int. Conf. Learn. Representations (ICLR)*, 2014.
- [51] I. Loshchilov and F. Hutter, “SGDR: stochastic gradient descent with restarts,” *Int. Conf. Learn. Representations (ICLR)*, 2017.
- [52] D. Gehrig, M. Gehrig, J. Hidalgo-Carrió, and D. Scaramuzza, “Video to Events: Recycling video datasets for event cameras,” in *IEEE Conf. Comput. Vis. Pattern Recog. (CVPR)*, 2020.
- [53] H. Rebecq, D. Gehrig, and D. Scaramuzza, “{ESIM}: an Open Event Camera Simulator,” *Conf. on Robotics Learning (CoRL)*, 10 2018.
- [54] M. Mostafavi, L. Wang, and K.-J. Yoon, “Learning to reconstruct hdr images from events, with applications to depth and flow prediction,” *International Journal of Computer Vision*, vol. 129, no. 4, pp. 900–920, 2021.
- [55] A. Paszke, S. Gross, S. Chintala, G. Chanan, E. Yang, Z. DeVito, Z. Lin, A. Desmaison, L. Antiga, and A. Lerer, “Automatic differentiation in pytorch,” in *NIPS-W*, 2017.
- [56] J. Schulman, F. Wolski, P. Dhariwal, A. Radford, and O. Klimov, “Proximal policy optimization algorithms,” *arXiv preprint arXiv:1707.06347*, 2017.
- [57] B. Zhou, F. Gao, L. Wang, C. Liu, and S. Shen, “Robust and efficient quadrotor trajectory generation for fast autonomous flight,” *IEEE Robotics and Automation Letters*, vol. 4, no. 4, pp. 3529–3536, 2019.
- [58] P. Florence, J. Carter, and R. Tedrake, “Integrated perception and control at high speed: Evaluating collision avoidance maneuvers without maps,” in *Algorithmic Foundations of Robotics XII: Proceedings of the Twelfth Workshop on the Algorithmic Foundations of Robotics*. Springer, 2020, pp. 304–319.